# Carbon onion / sulfur hybrid cathodes via inverse vulcanization for lithium sulfur batteries

Soumyadip Choudhury, Pattarachai Srimuk, Kumar Raju, Aura Tolosa, Simon Fleischmann, Marco Zeiger, Kenneth I. Ozoemena, Lars Borchardt and Volker Presser

*Sustainable Energy Fuels 2(2018), 133-146*



# Carbon onion / sulfur hybrid cathodes via inverse vulcanization for lithium sulfur batteries

**Soumyadip Choudhury,[1] Pattarachai Srimuk,[1,2] Kumar Raju,[3] Aura Tolosa,[1,2] Simon Fleischmann,[1,2] Marco Zeiger,[1,2] Kenneth I. Ozoemena,[4] Lars Borchardt,[5] and Volker Presser[1,2,*]**

[1] INM - Leibniz Institute for New Materials, Campus D2 2, 66123 Saarbrücken, Germany

[2] Department of Materials Science and Engineering, Saarland University, Campus D2 2, 66123 Saarbrücken, Germany

[3] Council for Scientific and Industrial Research, Brumeria Road, 0001 Pretoria, South Africa

[4] Molecular Sciences Institute, School of Chemistry, University of the Witwatersrand, Johannesburg 2050, South Africa

[5] Department of Inorganic Chemistry, Technische Universität Dresden, Bergstraße 66, 01062 Dresden, Germany

* Corresponding author: volker.presser@leibniz-inm.de

**Keywords**: lithium-sulfur batteries; carbon onions; polysulfides; rechargeable batteries

## Abstract

A sulfur-1,3-diisopropenylbenzene copolymer was synthesized by ring-opening radical polymerization and hybridized with carbon onions at different loading levels. The carbon onion mixing was assisted by shear in a two-roll mill to capitalize on the softened state of the copolymer. The sulfur copolymer and the hybrids were thoroughly characterized in structure and chemical composition, and finally tested by electrochemical benchmarking. A large enhancement of specific capacity was observed up to 140 cycles at higher content of carbon onions in the hybrid electrodes. The copolymer hybrids demonstrate maximum initial specific capacity of 1150 $mAh \cdot g^{-1}_{sulfur}$ (850 $mAh \cdot g^{-1}_{electrode}$) and a low decay of capacity to reach 790 $mAh \cdot g^{-1}_{sulfur}$ (585 $mAh \cdot g^{-1}_{electrode}$) after 140 charge/discharge cycles. All carbon onion / sulfur copolymer hybrid electrodes yielded high chemical stability, stable electrochemical performance superior to a conventional melt-infiltrated reference samples having similar sulfur and carbon onion content. The amount of carbon onions embedded in the sulfur copolymer has a strong influence on the specific capacity, as they effectively stabilize the sulfur copolymer and sterically hindered recombination of sulfur species to $S_8$ configuration.

## 1. Introduction

Among the various rechargeable battery systems, lithium-ion batteries offer one of the highest specific energies and their use in devices for mobile communication or electric cars is widespread.[1] While next-generation battery technologies, such as Li-S and Li-air, show promises towards enhancing the specific energy level, their long term cycle stability is still a remaining issue.[2] Theoretically, Li-S batteries are capable of delivering a high specific capacity of 1675 $mAh \cdot g^{-1}_{sulfur}$ and a high specific energy of up to 600 Wh/kg on a device level; however, the long-term cycle performance is affected by the insulating character of sulfur, the dissolution of polysulfide reaction intermediates, the shuttle effect, and lithium metal passivation.[3] To capitalize on the high specific capacity, high natural abundance, and low cost of sulfur as electrochemically active material, vast research efforts are being undertaken worldwide.

A key issue of Li-S cathode design is to ensure a high level of sulfur utilization. There are numerous works on the design of carbon as effective substrates for sulfur in order to maximize the sulfur utilization and to minimize the capacity fading.[3-5] Among the different conductive carbons, researchers have investigated multi-walled carbon nanotubes,[6-8] graphite and its derivatives,[9-11] mesoporous carbon,[12] carbide-derived carbon,[13] bio-sourced carbon,[14, 15] three-dimensionally ordered carbon with bi-continuous gyroidal morphology,[16, 17] activated carbon fiber cloth,[18] soft-templated[19] and hard-templated carbons[20] to embed sulfur for Li-S batteries. In our previous study, we have introduced carbon onion / sulfur hybrid electrodes;[21] the exclusively outer porosity of carbon onions enabled a high sulfur loading and high degree of active sulfur utilization.[21]

A promising strategy to enhance the electrochemical performance of a Li-S device is to manipulate the sulfur carrier. Xin et al.[22] reported that smaller sulfur molecules such as $S_{2-4}$ promise better electrochemical performance than the $S_8$-ring because these smaller sulfur molecules can fully avoid the unfavorable transformation of $S_8$ to $S_4^{2-}$. By this way, the formation of soluble polysulfide intermediates can be eliminated, and the smaller sized sulfur molecules can be efficiently confined inside carbon nanopores. Another way to develop sulfur carriers is to use an elemental sulfur melt as a feedstock for a ring-opening radical copolymerization with vinyl monomers.[23-25] This method yields a chemically stable copolymer with high sulfur content. Simmonds et al.[23] introduced an alternative to conventional vulcanization processes where sulfur is typically linked to double-bonds of the

elastomer chains.[26] During inverse vulcanization, sulfur is chemically linked to vinyl monomers. These chemically stabilized copolymers suppress the dissolution of polysulfides into the electrolyte, while still serving as an effective sulfur source for Li-S cathodes. Several vinyl monomers can form stable copolymers with sulfur, for example, 1,4-diphenylbutadiyne,[24] 1,10-(methylenedi-4,1-phenylene)bismaleimide,[27] or divinylbenzene.[25] In previous works, a vitrified copolymer was ground and mixed with carbon black to obtain carbon-sulfur cathodes.[23, 24, 27] In 2017, Hu et al. used carbon nanotubes, grown on anodic aluminum oxide discs, as hosts for a sulfur-rich copolymer (sulfur-*co*-1,3-diisopropenylbenzene).[28] Thereby, a sulfur mass loading of 63.5 % was obtained; yet, the fast vitrification of this copolymer prevents the facile mixing with porous carbon in the fluid state.

In this work, we explore carbon onions as hosts for a sulfur-rich copolymer synthesized via inverse vulcanization of sulfur and 1,3-diisopropenylbenzene (DIB). We chose carbon onions because of their high electronic conductivity, large external surface area, and small primary particle size below 10 nm, which allows for a nanoscale intertwining of carbon and sulfur.[29, 30] These properties benefit the formation of a hybrid material, that is, chemical linking of the two components on a nanoscale, rather than a composite by simple mechanical admixing of the conductive carbon component.[31] This strategy of hybridization was found to offer beneficial electrochemical performance in past works.[32] The processing of the sulfur-rich copolymer with carbon onions under high shear facilitates intricate mixing of the components without altering the consolidated nanostructures of carbon onions considerably. Thus, it enables electrochemical accessibility of large fractions of sulfur. Combining inverse vulcanization, highly electrically conducting carbon onion substrate with high external surface area, and shear-assisted mixing result stable Li-S battery cathodes. These electrodes were thoroughly characterized and electrochemically benchmarked, showing promising performance of 790 $mAh \cdot g^{-1}_{sulfur}$ (585 $mAh \cdot g^{-1}_{electrode}$) after 140 charge/discharge cycles (initially: 1150 $mAh \cdot g^{-1}_{sulfur}$, 850 $mAh \cdot g^{-1}_{electrode}$).

## 2. Experimental description

### 2.1. Materials

Nanodiamond powder was purchased from NaBond Technologies. Elemental sulfur ($S_8$), polyvinylidene fluoride (PVDF) of molar mass ca. 534 kg·mol$^{-1}$, *N*-methyl-2-pyrrolidone (NMP), bis(trifluoromethane)sulfonimide lithium salt (LiTFSI), lithium nitrate ($LiNO_3$), 1,2-dimethoxyethane (DME) and 1,3-dioxolane (DOL) were purchased from Sigma Aldrich. 1,3-diisopropenylbenzene was procured from TCI Deutschland GmbH. Nickel foil of thickness 13 µm was procured from Schlenk Metallfolien GmbH. Electrochemical grade high purity (99.9 %) lithium was purchased from PI-Kem. A microporous trilayer polypropylene-polyethylene-polypropylene (PP-PE-PP) separator membrane was obtained from Celgard (thickness: 25 µm). Non-woven PP separators (thickness: 150 µm) were provided by Freudenberg.

Carbon onions (abbreviated as onion-like carbon, OLC, for sample labeling) were synthesized from detonation nanodiamond by thermal annealing.[29] The nanodiamond particles had a typical diameter of 4-6 nm. The nanodiamond powder was annealed in argon atmosphere in a graphite crucible using a water-cooled high temperature furnace with tungsten heater (Thermal Technology) at 1700 °C for 1 h (heating/cooling rate: 20 °C·min$^{-1}$).[33]

The synthesis process is schematically depicted in **Fig. 1**. Elemental sulfur (3.6 g, 14 mmol) was heated to 130 °C. Magnetic stirring was started when sulfur was molten and then the temperature was raised to 185 °C. 400 mg (2.53 mmol) of 1,3-diisopropenylbenzene (DIB) was quickly injected into the reaction mixture. Immediately, the solution's color changed to deep orange and the rise of viscosity indicates the formation of semi-gelled copolymer. The copolymer is abbreviated as S-DIB. This gelled copolymer was immediately mixed with carbon onion to prepare hybrids before the vitrification occurred.

Carbon onion-sulfur hybrids with varied composition were prepared taking the S-DIB copolymer as sulfur source (**Table 1**). The copolymer hybrids with OLCs are abbreviated as S-DIB-OLC-*x* (*x* stands for the OLC loading in mass%). For comparison, melt-blended carbon onion / sulfur hybrid cathodes as reference material were prepared following the same composition. The sulfur hybrids by melt-blending with OLCs are abbreviated as S-OLC-*x* (*x* stands for the OLC loading in mass%). No additional conductive additive (like carbon black) was used since carbon onions are already highly conductive.[30] By this way, we achieved maximum sulfur loading of 79 mass% in the final electrode. The as-prepared semi-gelled

sulfur copolymer was immediately mixed with requisite amount of OLC in a two-roll mill to achieve a uniform dispersion of OLC in the copolymer. Later, the mixture was thermally annealed at 185 °C for 10 min. The mixture was cooled to room temperature and ground to fine powder for preparing the electrode slurry. For the control samples, the carbon onion / sulfur hybrid powder was thermally annealed at 155 °C for 5 h in an oven under argon atmosphere. After thermal treatment, the sample material was cooled under argon to room temperature and manually ground in a mortar to obtain a fine powder.

### 2.2. Electrode fabrication

Carbon onion / sulfur hybrid powders were mixed with 5 mass% of polyvinylidene fluoride (PVDF) binder in *N*-methyl-2-pyrrolidone (NMP). The resulting cathode slurry was coated onto a sheet of nickel current collector and was dried at room temperature overnight and in an oven at 60 °C to remove the remaining solvent. The dry electrode thickness was 100±20 µm with a mass loading of 4-6 $mg \cdot cm^{-2}$, which is equivalent to sulfur loading of 3-5 $mg \cdot cm^{-2}$. Thick electrodes of such mass loadings are necessary to attain desired areal capacity for automotive application of such batteries.[34]

### 2.3. Material characterization

Raman spectra were recorded by a Renishaw inVia Raman Microscope employing an Nd:YAG laser with an excitation wavelength of 633 nm. A grating with 1800 $lines \cdot mm^{-1}$ and a 50x objective (numeric aperture: 0.9) was used to reach a spectral resolution of about 1.2 $cm^{-1}$. The laser spot on the sample was about 1 µm in diameter at a power of 0.2 mW at the focal point. The acquisition time of each spectrum was 30 s and 50 accumulations were recorded.

The Raman spectra of carbon onion and the hybrids were deconvoluted using four Gaussian profiles.[35] Each spectrum was fitted within the characteristic carbon region (1000-1800 $cm^{-1}$) to signals of amorphous and graphitic carbon. The crystalline structure of the carbon-sulfur hybrids was analyzed by X-ray diffraction employing a X'PERT MPD system from PANalytical with a copper X-ray source ($Cu_{K\alpha}$, 40 kV, 40 mA). The measurements were recorded in the angle range of 10-60 °2θ.

Porosity analysis of carbon onions was conducted in Autosorb iQ nitrogen gas sorption system from Quantachrome. The carbon onion power was first degassed at 300 °C under vacuum ($10^{-2}$ Pa) for 10 h. The gas sorption measurement was carried out at liquid nitrogen

temperature (-196 °C) in 68 steps within the relative pressure range of $5 \cdot 10^{-7}$ to 1.0. The pore size distribution was derived from quenched-solid density functional theory (QSDFT) considering a slit-shaped pore geometry.[36, 37] The Brunauer-Emmett-Teller surface area (BET-SSA) was calculated in the linear regime of the isotherms from 0.1-0.3 $P/P_0$.[38] The gas sorption measurements of S-DIB-OLC samples were recorded following the same relative pressure ranges. Before inserting the hybrid samples into the gas sorption measurement device, they were degassed at 80 °C for 20 h under vacuum. A lower temperature and longer duration for degassing were chosen to avoid melting as well as to avoid thermal ageing of the copolymer. The gas sorption measurements (GSA) of melt hybridized S-OLC samples were not measured as elemental sulfur sublimes during degassing before placing the GSA cells for measurements.

$^1$H nuclear magnetic resonance (NMR) spectra of 1,3-diisopropenylbenzene (DIB) and sulfur-DIB copolymers were recorded using a Avance III HD Nanobay 300 MHz spectrometer. Small quantities of samples were dissolved in deuterated chloroform ($CDCl_3$) for NMR analysis. Chemical shifts are referenced to tetramethylsilane ($Me_4Si$, $\delta$ = 0 ppm).

Differential scanning calorimetry thermograms were recorded under continuous flow of nitrogen using a DSC 1 system from Mettler Toledo ANALYTICAL in combination with the STAR software using standard aluminum crucibles (40 µL). The scan rate for all thermograms was 10 °C·min$^{-1}$.

We used thermogravimetric analysis (TGA) to quantify the sulfur mass loading in each carbon onion / sulfur hybrid electrode. As sulfur sublimes when heating to 500 °C; TGA of the carbon-sulfur hybrids were performed in Netzsch Libra TG 209 F1 equipment in the temperature range at 30-500 °C with a heating rate of 10 °C·min$^{-1}$ under continuous flow of argon. In addition, the amount of sulfur was measured by CHNS elemental analysis technique with a Vario Micro Cube system (Elementar Analysensysteme). After combustion, the samples were measured under oxygen at 1150 °C in a tin holder. The CHNS analyzer was calibrated with sulfanilamide using different masses (41.6 mass% C, 4.1 mass% H, 8.1 mass% N, 18.5 mass% S).

Scanning electron micrographs of the carbon-sulfur hybrids were captured with a FEI SEM system operated with an acceleration voltage of 3 kV. Elemental maps were recorded at 10 kV in the same instrument fitted with Versa 3 EDX detector. No conductive sputtering

was necessary as all our samples were sufficiently conducting to acquire images without charging interferences.

Transmission electron micrographs were captured on JEOL JEM-2100F system operated at 200 kV. EDX mapping was performed using a Thermo Scientific MC100021 detector attached to the TEM chamber also with 200 kV and acquisition time for mapping was 10 min. The specimen was prepared by dispersing the hybrid powder in ethanol followed by placing a drop on a lacey carbon film copper grid.

The electrical conductivity of the hybrid electrodes was measured by casting electrode slurries on 50 µm flat polyimide film. The thicknesses of the electrodes were kept same as for the electrodes on nickel current collector (100±20 µm). Sheet resistances were measured with a custom-built spring-loaded four-point probe with blunt gold contacts (tip diameter: 1.5 mm, distance between two successive tips: 3 mm).

For post mortem analysis, the 2032-type coin cells were disassembled in the charged state. The electrodes were first washed several times with DME/DOL 1:1 (by volume). Then, the electrode materials from the disassembled cells were peeled off and few grains of them were dispersed in ethanol individually. Later, samples were prepared by adding one drop of the dispersion on the TEM grid.

We also performed the post mortem analysis by $^{1}H$ nuclear magnetic resonance spectroscopy of the electrodes after $100^{th}$ galvanostatic cycle at 0.1C rate. The cells were disassembled, and the hybrid cathodes were dissolved in deuterated dichloromethane ($CD_2Cl_2$) solvent. The carbon was filtered off by using 0.2 µm PTFE syringe filter and the solution was transferred to glass tubes for $^{1}H$ NMR measurements.

### 2.4. Electrochemical analyses

Disc cathodes of 15 mm were punched and 2032-type coin cells were assembled in an argon filled glove box (MBraun, $O_2$, $H_2O$ <1 ppm) with carbon onion / sulfur cathodes and lithium metal anodes. Prior to closing the cell, the separators were soaked with 50 µL of 1 M LiTFSI + 0.25 M $LiNO_3$ in 1:1 (by volume) 1,2-dimethoxyethane (DME) and 1,3-dioxolane (DOL) electrolyte. The electrolyte-to-sulfur ratio plays an important role to achieve ultimate cell performance;[39] therefore, the electrolyte-to-sulfur ratio for our measurements was kept in the range of 9-10 $mL \cdot g^{-1}$.

Cyclic voltammetry was performed with a Biologic VPM-300 potentiostat-galvanostat in a 3-electrode setup in a custom-made PEEK (polyether ether ketone) cell in the potential range of +1.7 V to +2.8 V vs. $Li^+/Li$ at a scan rate of 0.1 $mV \cdot s^{-1}$. A 3-electrode cell-configuration was adopted for cyclic voltammetry to observe any changes of the redox peak positions in different cycles due to SEI formation and effect of polysulfide shuttle on metallic lithium counter electrode. For cyclic voltammetry experiments, 12 mm disc electrodes and 13 mm separators were used. We used 40 µL of electrolyte to soak the separators. A small wire of lithium was introduced from the side as reference electrode. The reference lithium was separated by a glass fiber separator piece to avoid the electrical contacts with the working and counter electrode. Galvanostatic charge/discharge cycling were carried out in Maccor 96 channel battery analyzer at a constant current density of 336 $mA \cdot g^{-1}$ (0.2 C) for charging and 168 $mA \cdot g^{-1}$ (0.1 C) for discharging in the potential window of +1.8 V to +2.6 V vs. $Li^+/Li$. Rate capability benchmarking was carried out with a Maccor 96 channel battery analyzer at a constant charging rate of 0.2 C and 0.1 C for discharging was set for the first 20 cycles. Then, charging/discharging rates of 0.4 C/0.2 C, 1 C/0.5 C and 2 C/1 C were programmed in steps of 10 cycles. After 50 cycles, the 0.2 C/0.1 C charging/discharging rate was re-established to run the experiment until 75 cycles were completed.

## 3. Results and discussions

### 3.1. Structure, morphology, and chemical composition

When sulfur is heated above the temperature of the ring-opening polymerization (185 °C), it forms radicals which initiate a copolymerization reaction.[23] It forms a random copolymer with DIB (S-DIB) via bulk polymerization. It is the challenge to manufacture a sulfur source with a high sulfur content, which can be reversibly extracted during the Li-S battery operation. On the one hand, too little amount of DIB (for example, 5 mass%) in the copolymer forms sparingly soluble sulfur species. Neither stable electrodes nor a stable electrochemical performance can be achieved by this. On the other hand, a higher amount of DIB (over 10 mass%) leads to the creation of organosulfur units with a high organic content resulting in high solubility in organic electrolytes.[23] Based on the work by Simmonds et al.[23], we chose a co-monomer feed ratio of sulfur and DIB of 9:1 (by mass) to achieve the optimized effect of DIB addition to sulfur on the performance of Li-S battery cathodes. The formation of the copolymer was confirmed by $^1H$ NMR (**Fig. 2A**). The NMR signals of DIB in

the range of 7.2-7.6 ppm δ are related to the protons of the aromatic rings. The peaks at 5-5.4 ppm δ are attributed to the protons adjacent to the double bond of the side groups. The protons from methyl groups next to vinyl group are visible at 2.2 ppm δ. As can be seen, the signal from the protons of the vinyl monomer units completely disappeared (at 5-5.4 ppm δ) after copolymerization and a new set of peaks appeared at 0.6-1.8 ppm, which are correlated to the protons from the methyl (-$CH_3$) and methylene (-$CH_2$-) groups adjacent to the sulfur linkage. The aromatic proton intensities at 7.2-7.6 ppm δ in S-DIB copolymer are very low due to the predominance of the methyl and methylene proton intensities. This finding confirms the complete transformation of co-monomers without any residual monomer content.

The materials were further characterized by differential scanning calorimetry to characterize the thermal behavior of the neat copolymer and to notice the differences upon addition of carbon onions. The thermogram of the neat copolymer shows a glass transition temperature ($T_g$) at -23.4 °C (**Fig. 2B**). The appearance of a single glass transition temperature in DSC thermogram indicates the formation of a random copolymer of sulfur and DIB. As the glass transition temperature is below room temperature, the copolymer is in a softened state allowing to be processed with carbon onions in a two-roll mill at ambient conditions. The values for $T_g$ shift towards higher temperatures relative to the neat copolymer for higher amounts of carbon onions. This is possibly due to the restricted chain mobilities of the copolymer by carbon onion addition. The $T_g$ goes up to a maximum value of -8.3 °C at 30 mass% OLC addition to the copolymer. Besides the $T_g$ peak, there are also clear melting and re-crystallization peaks for all hybrid materials. The peak intensities were decreased with progressive addition of OLC into the hybrid possibly due to the inclusion of the OLCs between the chains of copolymers, which restrict the orientation of the chains during the shear-assisted mixing.

In our study, we chose carbon onions obtained via annealing nanodiamonds at 1700 °C in argon as conductive substrate for sulfur copolymer.[40, 41] At this high temperature, $sp^3$-hybridized nanodiamond particles with a mean size of ca. 5 nm (**Fig. 3A**) transform to $sp^2$-hybridized carbon onions (**Fig. 3B**). During thermal annealing, the diamond lattices of 0.21 nm reorganize to a structure composed of concentric graphitic shells with layer spacing of 0.34 nm, yielding the multi-shell feature characteristics for carbon onions. The transmission electron micrographs also show that carbon onions with primary particle size of

5-10 nm are locally agglomerated. When carbon onions were added to the semi-gelled sulfur copolymer, a uniform and homogenous material was obtained (**Fig. 3C, Fig. 4,** and *Supporting Information* **Fig. S1**). The pristine carbon onions show a surface area of 430 $m^2 \cdot g^{-1}$ (BET) and 404 $m^2 \cdot g^{-1}$ (DFT) with a pore volume of 1.21 $cm^3 \cdot g^{-1}$ composed of micropores and mesopores (**Fig. 5A**), in between the particles. When sulfur-1,3-diisopropenylbenze copolymer was hybridized with different mass% of OLC, the pores around the OLCs were being covered with the S-DIB copolymers. There is clear indication that the available surface area as well as the pore volume significantly decreased by hybridization with S-DIB copolymers. With high loadings of S-DIB copolymers to the OLC (S-DIB-OLC-10 and S-DIB-OLC-20), the surface area significantly dropped to 11-16 $m^2 \cdot g^{-1}$ (BET) with almost no micropores accessible according to GSA measurements (*Supporting Information* **Fig. S2, Table S1**). In the S-DIB-OLC hybrid with highest amount of OLC loading (S-DIB-OLC-30), the surface area reduced to 43 $m^2 \cdot g^{-1}$ (BET), and still a small fraction of micropore volume was incompletely filled by the S-DIB copolymers. This possibly allows better wetting of the electrodes by the electrolyte and better $Li^+$ ion transport throughout the hybrid cathodes.

The elemental maps from TEM-EDX reveal an inhomogeneous distribution of carbon onions in the sulfur copolymer phase for samples containing a high amount of sulfur (**Fig. 4A**), whereas the sulfur tends to be distributed more homogeneously with higher amounts of carbon onions (**Fig. 4B-C**). The melt-infiltrated hybrids showed a similarly good distribution in EDX (*Supporting Information* **Fig. S3**). SEM-EDX elemental maps of copolymer hybrids also demonstrate an overview of the distributions of carbon and sulfur like TEM-EDX observations (*Supporting Information* **Fig. S4**).

From thermogravimetric analysis (TGA) in inert atmosphere, we quantified the amount of sulfur in the hybrid electrodes. In non-oxidizing environments, carbon onions undergo very little mass loss (ca. 1 mass%) which can be attributed to the decomposition of the (few) functional surface groups. The carbon onion / sulfur copolymer hybrid and carbon onions / sulfur hybrid (reference sample) materials demonstrate a single-step mass loss, which started at 240 °C and was completed at 500 °C (**Fig. 5B**), indicative of sulfur evaporation. The sulfur content of 63-83 mass%, determined from thermogravimetry is in alignment with the sulfur content determined from CHNS analysis (**Table 2**).

Next, we measured the Raman spectra of carbon onions, sulfur, S-DIB, and their corresponding hybrids (**Fig. 5C**, **Table 3**). The Raman spectra of carbon onions show a D-band at 1338 $cm^{-1}$, G-band centered at 1580 $cm^{-1}$, and a higher order and combinational modes at around 2700 $cm^{-1}$ (**Fig. 5C**).[42] The G-band originates from $sp^2$-hybridized carbon in rings and the D-band is typical of incompletely graphitic materials in the presence of defects.[43, 44] The positions of the D- and G-bands shift to significantly higher frequencies compared to the pristine carbon onion powder after hybridization with sulfur via milling (from 1323 $cm^{-1}$ to 1340-1342 $cm^{-1}$ and from 1596 $cm^{-1}$ to 1608-1610 $cm^{-1}$). This is indicative of a reduction in graphitic ordering caused by (1) mechanical stresses during milling, and (2) the formation of a sulfur / carbon interface, as it was observed in other works.[45] Sulfur shows three Raman bands at 156 $cm^{-1}$, 219 $cm^{-1}$, and 473 $cm^{-1}$, which are attributed to S-S bond vibrations.[14, 21, 46] The sulfur copolymer also showed similar Raman peaks at the characteristic sulfur positions. In all carbon onion / sulfur hybrids prepared by melt-infiltration, we observe clearly visible sulfur bands. In the S-DIB-OLC samples, the sulfur bands become less prominent with progressive addition of carbon onions. This is possibly due to the tighter nanoscale intertwining with carbon onions and smaller domain sizes of sulfur in the copolymer.

To assess the crystalline structure of the samples, we carried out X-ray diffraction (**Fig. 5D**). Carbon onions present a very broad peak centered at 26° 2θ position. The broad graphitic (002) peak is due to the incompletely crystalline carbon onions of below 10 nm primary particle size. The elemental sulfur peaks recorded are in alignment with reference data (PDF 78-1889). The sulfur copolymer does not show sulfur peaks at 23° 2θ because sulfur is no longer present in $S_8$ configuration. A new XRD pattern with its main reflections at 19° and 24° 2θ is visible, indicative of polymer and sulfur chain ordering. The sulfur copolymer represents broadened X-ray reflections which can be correlated to the reduced long-range order by the bridging of the sulfur backbone with DIB units.[28] Carbon onion / sulfur copolymer hybrids show different diffractograms, with S-DIB-OLC-10 and S-DIB-OLC-20 containing several characteristic $S_8$ signals; for example, the main reflection at around 23 °2θ, whereas S-DIB-OLC-30 resembles the diffractogram of S-DIB copolymer. This suggests that sulfur in $S_8$ configuration precipitates to some extent when hybridizing with small amounts of carbon onions (10-20 mass%) during the milling process. When using 30 mass% of carbon onions, the sulfur copolymer structure remains mostly unchanged. This is possibly caused by the larger amounts of carbon onions that sterically inhibit recombination of sulfur chains to $S_8$ configuration.

The resulting conductivity for sulfur and sulfur-containing copolymer hybrids was assessed by sheet resistance measurements with a four-point probe (**Table 4**). There are little improvements of conductivities between hybrids obtained from the sulfur copolymer and from the elemental sulfur reference sample via melt infusion when comparing the same level of mass loading with carbon onions; the highest value of conductivity was obtained at 30 mass% carbon onion loading (0.31-0.36 $S \cdot cm^{-1}$). This is expected since the conductivity is mainly caused by homogenously distributed carbon onions forming conductive pathways, whereas the aromatic π-electron cloud of the sulfur copolymer might be responsible for the slightly enhanced conductivity compared to the $S_8$ system having similar carbon onion content.[28, 47]

### 3.2. Electrochemical performance

The electrochemical performance was evaluated by cyclic voltammetry (3-electrode set-up) and galvanostatic cycling under potential limitations (2-electrode set-up). The cyclic voltammograms show typical sulfur reduction and oxidation steps (**Fig. 6A,C,E**).[18, 48-50] During discharging, two characteristic sulfur peaks occurred at +2.3 V and +1.98 V vs. $Li^+/Li$. The first reduction peak at +2.2 V vs. $Li^+/Li$ shifted by +0.8 V in the subsequent cycles, which might be due to the stabilization of the cell in first cycle and reduced electrode polarization.[10, 51] The first reduction peak corresponds to the formation of the longer Li-organosulfur units ($Li_2S_n$) and $Li_2S_8$.[12, 23, 28] Further reduction of these species leads to the formation of lower order of organosulfur species (n > 4) and finally to $Li_2S_2$ and $Li_2S$ at the potential of ca. +2 V vs. $Li^+/Li$. During the oxidation process, two overlapping peaks for conversion of high and low order organo-polysulfide units appear. The peak positions for oxidation and reduction of the samples obtained from use of the sulfur copolymer are found similar with the conventional carbon-sulfur electrodes prepared by melt-infusion.[18, 49, 50] The only difference is the separation of the peak positions and the width of the redox peaks in the case of sulfur copolymer system compared to the melt-infused samples (*Supporting Information* **Fig. S5**). This is more clearly visible at high carbon onion loading with both sulfur filling methods. The relatively narrow peaks and similar peak positions with prolonged cycles are indicative of good reaction kinetics assisted by the conductive carbon onion substrate.[21] At low carbon onion loadings, there exist considerable amounts of electrochemically inactive sulfur located further away from the carbon onion surfaces. This also hinders the $Li^+$ ion diffusion through the electrode. For that reason, the specific current response for highest sulfur loadings (**Fig. 6E**) is very low (ca. 700 $mA \cdot g^{-1}_{sulfur}$).

During reversible galvanostatic charge-discharge measurements, two characteristic plateaus for reduction and oxidations appear. The peak voltages from cyclic voltammetry and voltage plateaus from galvanostatic cycling exactly match with each other (**Fig. 6B,D,F**). As per the mechanism provided by Simmonds et al.,[23] both $S_8$ and S-DIB follow the similar electrochemical pathway demonstrating two-plateau behavior of normalized capacity vs. voltage profiles. S-DIB undergoes the redox reaction through oraganosulfur moieties. Initially, during discharge of S-DIB copolymers, the high voltage plateau regime at +2.3 V vs. $Li^+/Li$ can be assigned to the formation of higher order organosulfur units and $Li_2S_8$.[23, 24, 28] Upon further discharge, we identified another plateau at +2.1 V vs. $Li^+/Li$. This contributes to

a large degree to the total capacity with further reaction from higher order organosulfur units to shortened oligosulfur units and $Li_2S_4$. Continued discharge at the lower voltage plateau resulted due to the conversion of shortened oligosulfur units and $Li_2S_4$ into fully discharged organosulfur DIB products and insoluble mixtures of $Li_2S_3$ and $Li_2S_2$. According to the literature, this step is slow due to the slow reaction kinetics of lower order organosulfur units to finally insoluble sulfur species.[28] The voltage plateaus occur at the same potential with extended battery cycling which reflects the slow rate of capacity decay with higher number of duty cycles.

The specific capacities normalized to the sulfur mass vs. cycle number were presented in **Fig. 7A,B**. In most of the published reports, either a low sulfur loading or thin electrodes were tested. It is not clear whether the approaches adopted for thin-film sulfur electrodes can equally work when the cathode thickness is significantly increased. For real applications of high energy density batteries, sulfur loading as high as 70 mass% is necessary and the areal loading of sulfur should be at least 2-3 $mg \cdot cm^{-2}$ to be considered for automotive applications.[34] Several approaches to enhance the areal capacities are reported, for example, by stacking multiple layers of CNT paper electrodes,[52] sulfur melt infiltrated 3-D vertically aligned nanoflakes derived from reduced graphene oxide,[53] sandwich structure of sulfur between two different current collectors,[54] or layer-transferred vertically aligned CNT films[55]. A comparison of specific capacities with different areal loading of sulfur from the literature with different types of carbon substrates is presented in **Table 5**. The carbon onion / sulfur copolymer hybrid with 30 mass% carbon onion loading demonstrates an initial specific capacity of 1150 $mAh \cdot g^{-1}_{sulfur}$ (3.45 $mAh \cdot cm^{-2}$). After 3 cycles, the specific capacity value reached to 1050 $mAh \cdot g^{-1}_{sulfur}$ (3.15 $mAh \cdot cm^{-2}$), afterwards a small rate of capacity fading was noticed. At the $100^{th}$ cycle, the retained capacity was 880 $mAh \cdot g^{-1}_{sulfur}$ (2.64 $mAh \cdot cm^{-2}$). The discharge capacity obtained from other carbon onion / sulfur copolymer hybrids are 840 $mAh \cdot g^{-1}_{sulfur}$ (3.36 $mAh \cdot cm^{-2}$) at the $1^{st}$ cycle and 580 $mAh \cdot g^{-1}_{sulfur}$ (2.32 $mAh \cdot cm^{-2}$) at the $100^{th}$ cycle for S-DIB-OLC-20, or 380 $mAh \cdot g^{-1}_{sulfur}$ (1.9 $mAh \cdot cm^{-2}$) at the $1^{st}$ cycle and 270 $mAh \cdot g^{-1}_{sulfur}$ (1.35 $mAh \cdot cm^{-2}$) at $100^{th}$ cycle for S-DIB-OLC-10. The specific capacity values for the $1^{st}$ and $100^{th}$ cycles for all carbon onion / sulfur hybrids are presented in **Table 6**.

Compared to these values, the initial capacities of carbon onion / sulfur reference samples (S-OLC) are much lower and the specific capacities faded strongly during continued cycling.

The melt-infiltrated carbon onion / sulfur hybrid with 30 mass% carbon onion loading demonstrates an initial specific capacity of 915 $mAh \cdot g^{-1}_{sulfur}$ (2.75 $mAh \cdot cm^{-2}$). Within 3 cycles, the specific capacity value reached to 800 $mAh \cdot g^{-1}_{sulfur}$ (2.64 $mAh \cdot cm^{-2}$), afterwards a drastic rate of capacity fading was observed. At the $100^{th}$ cycle, the retained capacity was 22 $mAh \cdot g^{-1}_{sulfur}$ (0.07 $mAh \cdot cm^{-2}$). The discharge capacity obtained from another carbon onion / sulfur melt-infiltrated hybrid (S-OLC-20) is 755 $mAh \cdot g^{-1}_{sulfur}$ (3.02 $mAh \cdot cm^{-2}$) at the $1^{st}$ cycle and 20 $mAh \cdot g^{-1}_{sulfur}$ (0.08 $mAh \cdot cm^{-2}$) at the $100^{th}$ cycle. The best performance stability among the melt-infiltrated samples was maintained by S-OLC-10 with an initial capacity of 490 $mAh \cdot g^{-1}_{sulfur}$ (2.45 $mAh \cdot cm^{-2}$), but a significant performance drop was seen after the $80^{th}$ cycle. We have expressed the specific capacity values from galvanostatic cycling by normalizing to the electrode mass excluding the binder (**Fig. 7C,D**). All sulfur copolymer samples demonstrate very stable specific capacity values relative to the values obtained at $3^{rd}$ cycle. This means that the sulfur rich copolymer system is effective in stabilizing the electrochemical performance irrespective of the extent of carbon onion loading compared to the system where elemental sulfur was melt-infiltrated into the pores of carbon onions. The π-electron clouds of the aromatic moiety of sulfur copolymer units increase the electronic conductivity of the hybrid electrodes.[28, 47] This can also be explained by the improved conductivity of the copolymer hybrids relative to the melt-infiltrated hybrids at the same carbon onion loading level (**Table 4**), and the specific current values of the CV diagrams (**Fig. 6A,C,E**, *Supporting Information* **Fig. S5**).

The Coulombic efficiencies for the S-DIB-OLC hybrids are typically around 97-99% throughout the cycle study in long term cycle performance as well in rate handling study (**Fig. 7C,E**). For comparison, none of the S-OLC hybrids showed stable Coulombic efficiency values (**Fig. 7D**, *Supporting Information* **Fig. S6**). This behavior can be explained by an integrated electrode structure with sulfur copolymer and OLC carbon onions. In the melt hybridized samples, high loading of sulfur and low binder content neither could retain the structural integrity, nor could maintain the electrical connectivity between the hybrid components.

The rate handling behavior of the carbon onion / sulfur copolymer and OLC-S hybrid electrodes was measured in 2032-type coin cells. The rate performance data are plotted with multiple specific currents starting from low rate for 20 cycles (0.2 C charge / 0.1 C discharge) with continued increments of specific currents up to 2 C charge / 1 C discharge in

stepwise manner for each 10 cycles and finally brought back to slow current rate of 0.2 C charge / 0.1 C discharge (**Fig. 7E**). The specific capacity was recovered close to the values of the initial 20 cycles after several current rate fluctuations. The carbon onion / sulfur hybrids prepared via melt-diffusion technique showed very poor rate performance especially at higher C-rates (*Supporting Information* **Fig. S6**). From the capacity retention ability, it can be concluded that the carbon onion / sulfur integrated structure remained similar and was not ruptured under vigorous current fluctuations.

To ascertain the stability of the S-DIB copolymer, $^{1}$H nuclear magnetic resonance spectra were recorded after 100 galvanostatic cycles (**Fig. 8**). The chemical shifts of copolymer structure after electrochemical measurements are clearly visible in the 0.6-1.75 ppm range. In addition, we could see a couple of new peaks at 2.17 and 2.29 ppm copolymer. These two peaks possibly arise from the formation of low molecular sulfur species (sulfides) by fragmentation of copolymer structure to some extent under electrochemical influence. These two peaks can be correlated to dimethyl sulfides ($H_3C$-S-$CH_3$) and ethylene sulfide ($(CH_2)_2$-S) respectively. From the post mortem $^{1}$H NMR analyses, it can be concluded that the S-DIB copolymer retains the same chemical structure after several cycles of electrochemical benchmarking and can serve as efficient sulfur source for the Li-S batteries.

To validate the retention of electrode integrity upon cycling, we also conducted post mortem TEM-EDX with the electrode after the 100$^{th}$ cycles. The cells were opened in the charged state to convert all lower-order polysulfides and solid $Li_2S_2$ and $Li_2S$ back to the organosulfur copolymer. From the EDX maps of carbon and sulfur presented in **Fig. 9**, we see that the carbon and sulfur maps overlap each other like the distribution of the electrode materials measured before electrochemical operation. The additional fluorine signals originate from the PVDF binder and possibly from leftover electrolyte salt. After cell disassembly, the electrodes and separators were photographed before the electrolyte solvents evaporated. We noticed that the separators from the cells with highest sulfur copolymer loading exhibit a stronger yellow color (*Supporting Information* **Fig. S7**). This means that the electrodes with highest sulfur copolymer loading are prone to leach highest amount of soluble polysulfides. This can originate from the inclusion of higher mass of carbon onions, which might have reduced the polysulfide leaching tendency to even higher level.

## 4. Conclusions

This report introduces carbon onions for the fabrication of carbon-sulfur hybrid cathode with sulfur loading as high as 79 mass%. Our study demonstrates the effectiveness of carbon onions as a conducting matrix for the sulfur containing copolymers. The sulfur carrier (sulfur-1,3-diisopropenylbenzene copolymer) was synthesized and hybridized in the softened state to facilitate carbon onion distribution. To achieve better contact with matrix and sulfur copolymer, hybridization was assisted by a two-roll mill. In the sulfur copolymer, sulfur is a part of the copolymer backbone which can be reversibly detached and re-deposited to make it analogous to the conventional carbon-sulfur electrode by melt-infusion. The advantage of using the sulfur copolymer is to prevent the formation of soluble polysulfide species and to reduce the binder amount to 5 mass%. The covalent nature of sulfur bonds retains the possibility to regenerate the chemical structure with prolonged cycling, and the π-electron clouds of the aromatic copolymer units to increase the overall electron or ion transfer rate. The mixing in the softened state under shear, and the presence of exclusively exterior surface of carbon onions eliminates the problems of traditional pore filling by sulfur melt. Carbon onion-sulfur copolymer system at 30 mass% carbon onion loading reached initial specific capacity of 1150 $mAh \cdot g^{-1}_{sulfur}$ (850 $mAh \cdot g^{-1}_{electrode}$). This hybrid exhibited low decay of capacity and reached 790 $mAh \cdot g^{-1}_{sulfur}$ (585 $mAh \cdot g^{-1}_{electrode}$) after 140 charge/discharge cycles. The other two hybrids with 20 mass% and 10 mass% carbon onion content could only achieve a lower initial discharge capacity of 840 $mAh \cdot g^{-1}_{sulfur}$ (705 $mAh \cdot g^{-1}_{electrode}$) and 380 $mAh \cdot g^{-1}_{sulfur}$ (350 $mAh \cdot g^{-1}_{electrode}$), respectively. All copolymer hybrids exhibited stable electrochemical performance compared to melt-infiltrated samples having similar sulfur and carbon onion content. Sulfur copolymers present excellent chemical stability, higher electrochemical cyclic stability, and attractive rate handling behavior, compared to elemental sulfur in carbon onion conductive matrix. In addition, our sulfur copolymer hybrids demonstrate high areal specific capacity of ca. 3.4 $mAh \cdot cm^{-2}$ due to high areal sulfur loading. Our study shows the major impact of carbon onions on the electrochemical performance of the hybrid material. Larger amounts of carbon onions stabilize the sulfur copolymer, leading to a higher specific capacity, even with respect to the whole electrode mass possibly by providing intimate contacts between carbon onions and the sulfur copolymer; thereby, more electrochemically active sulfur is available for the Li-S battery.

## Acknowledgments

This work was supported under the framework of CREATe-Network Project, Horizon 2020 of the European Commission (RISE Project No. 644013). Financial support from the German Federal Ministry of Education and Research (BMBF) within the Mechanocarb project (award number 03SF0498) is gratefully acknowledged by LB. The authors thank Prof. Eduard Arzt (INM) and Dr. Mkhulu Mathe (CSIR) for their continuing support. The kind support and technical assistance of Stefan Brück and Benjamin Krüner (both at INM) is acknowledged.

## References


1. B. Dunn, H. Kamath and J.-M. Tarascon, *Science*, 2011, **334**, 928-935.
2. P. G. Bruce, S. A. Freunberger, L. J. Hardwick and J.-M. Tarascon, *Nature Materials*, 2011, **11**, 19-29.
3. L. Borchardt, M. Oschatz and S. Kaskel, *Chemistry – A European Journal*, 2016, **22**, 7324-7351.
4. X. Ji and L. F. Nazar, *Journal of Materials Chemistry*, 2010, **20**, 9821-9826.
5. L. Borchardt, H. Althues and S. Kaskel, *Current Opinion in Green and Sustainable Chemistry*, 2017, **4**, 64-71.
6. J. Ma, Z. Fang, Y. Yan, Z. Z. Yang, L. Gu, Y. S. Hu, H. Li, Z. X. Wang and X. J. Huang, *Advanced Energy Materials*, 2015, **5**, 1500046.
7. K. Mi, Y. Jiang, J. K. Feng, Y. T. Qian and S. L. Xiong, *Advanced Functional Materials*, 2016, **26**, 1571-1579.
8. Y. Fu, Y. S. Su and A. Manthiram, *Angewandte Chemie*, 2013, **125**, 7068-7073.
9. S. Evers and L. F. Nazar, *Chemical Communications*, 2012, **48**, 1233-1235.
10. L. Ji, M. Rao, H. Zheng, L. Zhang, Y. Li, W. Duan, J. Guo, E. J. Cairns and Y. Zhang, *Journal of the American Chemical Society*, 2011, **133**, 18522-18525.
11. C. Tang, B. Q. Li, Q. Zhang, L. Zhu, H. F. Wang, J. L. Shi and F. Wei, *Advanced Functional Materials*, 2015, **26**, 577-585.
12. X. Ji, K. T. Lee and L. F. Nazar, *Nature Materials*, 2009, **8**, 500-506.
13. T. J. Lee, Y. Zhao, S. Thieme, H. Kim, M. Oschatz, L. Borchardt, A. Magasinski, W. I. Cho, S. Kaskel and G. Yushin, *Advanced Materials*, 2013, **25**, 4573-4579.
14. F. Chen, J. Yang, T. Bai, B. Long and X. Zhou, *Electrochimica Acta*, 2016, **192**, 99-109.
15. M. Raja, N. Angulakshmi and A. M. Stephan, *RSC Advances*, 2016, **6**, 13772-13779.
16. S. Choudhury, M. Agrawal, P. Formanek, D. Jehnichen, D. Fischer, B. Krause, V. Albrecht, M. Stamm and L. Ionov, *ACS nano*, 2015, **9**, 6147-6157.
17. J. G. Werner, S. S. Johnson, V. Vijay and U. Wiesner, *Chemistry of Materials*, 2015, **27**, 3349-3357.
18. R. Elazari, G. Salitra, A. Garsuch, A. Panchenko and D. Aurbach, *Advanced Materials*, 2011, **23**, 5641-5644.
19. M. Agrawal, S. Choudhury, K. Gruber, F. Simon, D. Fischer, V. Albrecht, M. Göbel, S. Koller, M. Stamm and L. Ionov, *Journal of Power Sources*, 2014, **261**, 363-370.
20. N. Jayaprakash, J. Shen, S. S. Moganty, A. Corona and L. A. Archer, *Angewandte Chemie International Edition*, 2011, **123**, 6026-6030.
21. S. Choudhury, M. Zeiger, P. Massuti-Ballester, S. Fleischmann, P. Formanek, L. Borchardt and V. Presser, *Sustainable Energy & Fuels*, 2017, **1**, 84-94.
22. S. Xin, L. Gu, N.-H. Zhao, Y.-X. Yin, L.-J. Zhou, Y.-G. Guo and L.-J. Wan, *Journal of the American Chemical Society*, 2012, **134**, 18510-18513.
23. A. G. Simmonds, J. J. Griebel, J. Park, K. R. Kim, W. J. Chung, V. P. Oleshko, J. Kim, E. T. Kim, R. S. Glass, C. L. Soles, Y. E. Sung, K. Char and J. Pyun, *ACS Macro Letters*, 2014, **3**, 229-232.
24. P. T. Dirlam, A. G. Simmonds, T. S. Kleine, N. A. Nguyen, L. E. Anderson, A. O. Klever, A. Florian, P. J. Costanzo, P. Theato and M. E. Mackay, *RSC Advances*, 2015, **5**, 24718-24722.
25. I. Gomez, D. Mecerreyes, J. A. Blazquez, O. Leonet, H. Ben Youcef, C. Li, J. L. Gómez-Cámer, O. Bundarchuk and L. Rodriguez-Martinez, *Journal of Power Sources*, 2016, **329**, 72-78.
26. A. Coran, *Journal of applied polymer science*, 2003, **87**, 24-30.

27. M. Arslan, B. Kiskan, E. C. Cengiz, R. Demir-Cakan and Y. Yagci, *European Polymer Journal*, 2016, **80**, 70-77.
28. G. Hu, Z. Sun, C. Shi, R. Fang, J. Chen, P. Hou, C. Liu, H.-M. Cheng and F. Li, *Advanced Materials*, 2017, **29**, 1603835.
29. M. Zeiger, N. Jäckel, V. N. Mochalin and V. Presser, *Journal of Materials Chemistry A*, 2016, **4**, 3172-3196.
30. N. Jäckel, D. Weingarth, M. Zeiger, M. Aslan, I. Grobelsek and V. Presser, *Journal of Power Sources*, 2014, **272**, 1122-1133.
31. J. J. Vilatela and D. Eder, *ChemSusChem*, 2012, **5**, 456-478.
32. S. Fleischmann, M. Zeiger, N. Jäckel, B. Krüner, V. Lemkova, M. Widmaier and V. Presser, *Journal of Materials Chemistry A*, 2017, **5**, 13039-13051.
33. M. Zeiger, N. Jäckel, D. Weingarth and V. Presser, *Carbon*, 2015, **94**, 507-517.
34. D. Lv, J. Zheng, Q. Li, X. Xie, S. Ferrara, Z. Nie, L. B. Mehdi, N. D. Browning, J. G. Zhang and G. L. Graff, *Advanced Energy Materials*, 2015, **5**, 1402290.
35. F. C. Tai, S. C. Lee, J. Chen, C. Wei and S. H. Chang, *Journal of Raman Spectroscopy*, 2009, **40**, 1055-1059.
36. X. Chen, E. Pomerantseva, P. Banerjee, K. Gregorczyk, R. Ghodssi and G. Rubloff, *Chemistry of Materials*, 2012, **24**, 1255-1261.
37. P. I. Ravikovitch, A. Vishnyakov and A. V. Neimark, *Physical Review E*, 2001, **64**, 011602.
38. S. Brunauer, P. H. Emmett and E. Teller, *Journal of the American chemical society*, 1938, **60**, 309-319.
39. S. S. Zhang, *Energies*, 2012, **5**, 5190-5197.
40. V. L. Kuznetsov, A. L. Chuvilin, Y. V. Butenko, I. Y. Mal'kov and V. M. Titov, *Chemical Physics Letters*, 1994, **222**, 343-348.
41. M. Zeiger, N. Jäckel, M. Aslan, D. Weingarth and V. Presser, *Carbon*, 2015, **84**, 584-598.
42. M. S. Dresselhaus, A. Jorio, M. Hofmann, G. Dresselhaus and R. Saito, *Nano Letters*, 2010, **10**, 751-758.
43. A. C. Ferrari, *Solid state communications*, 2007, **143**, 47-57.
44. A. C. Ferrari and D. M. Basko, *Nature nanotechnology*, 2013, **8**, 235-246.
45. S. Fleischmann, N. Jäckel, M. Zeiger, B. Krüner, I. Grobelsek, P. Formanek, S. Choudhury, D. Weingarth and V. Presser, *Chemistry of Materials*, 2016, **28**, 2802-2813.
46. A. T. Ward, *The Journal of Physical Chemistry*, 1968, **72**, 4133-4139.
47. H. Kim, J. Lee, H. Ahn, O. Kim and M. J. Park, *Nature Communications*, 2015, **6**, 7278.
48. M.-K. Song, E. J. Cairns and Y. Zhang, *Nanoscale*, 2013, **5**, 2186-2204.
49. J. Guo, Y. Xu and C. Wang, *Nano Letters*, 2011, **11**, 4288-4294.
50. G. Li, J. Sun, W. Hou, S. Jiang, Y. Huang and J. Geng, *Nature Communications*, 2016, **7**, 10601.
51. H. Al Salem, G. Babu, C. V. Rao and L. M. R. Arava, *Journal of the American Chemical Society*, 2015, **137**, 11542-11545.
52. Z. Yuan, H. J. Peng, J. Q. Huang, X. Y. Liu, D. W. Wang, X. B. Cheng and Q. Zhang, *Advanced Functional Materials*, 2014, **24**, 6105-6112.
53. D. Singh, N. Soin, S. Sharma, S. Basak, S. Sachdeva, S. Roy, H. Zanderbergen, J. McLaughlin, M. Huijben and M. Wagemaker, *Sustainable Energy & Fuels*, 2017, **1**, 1516-1523.
54. Y. Zhang, K. Li, H. Li, Y. Peng, Y. Wang, J. Wang and J. Zhao, *Journal of Materials Chemistry A*, 2017, **5**, 97-101.

55. J. Brückner, S. Thieme, H. T. Grossmann, S. Dörfler, H. Althues and S. Kaskel, *Journal of Power Sources*, 2014, **268**, 82-87.
56. F. Jin, S. Xiao, L. Lu and Y. Wang, *Nano Letters*, 2016, **16**, 440-447.
57. C. Liang, N. J. Dudney and J. Y. Howe, *Chemistry of Materials*, 2009, **21**, 4724-4730.

## Figures

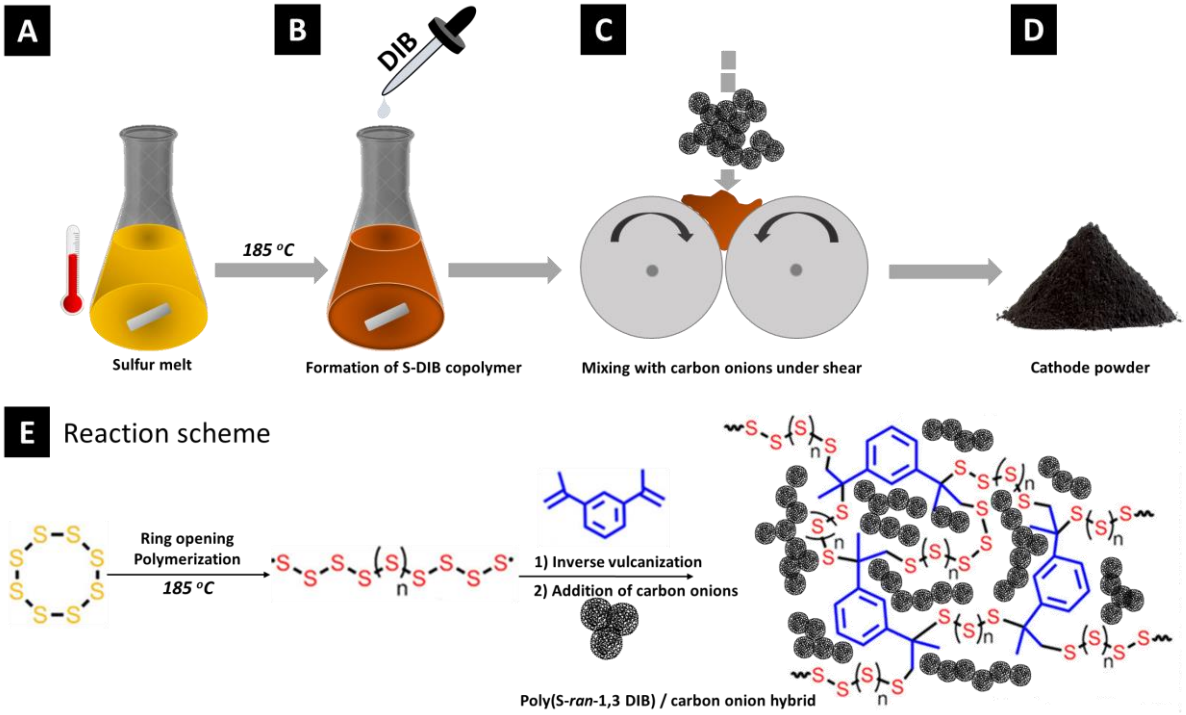


**Figure 1**: Schematic preparation of carbon onion / S-DIB copolymer hybrid material. (A, B) sulfur copolymer synthesis from sulfur melt upon addition of 1,3-diisopropenylbenzene (DIB), (C, D) carbon onion / sulfur copolymer hybrid preparation via two-roll mixing, and (E) reaction scheme for the sulfur copolymer synthesis.

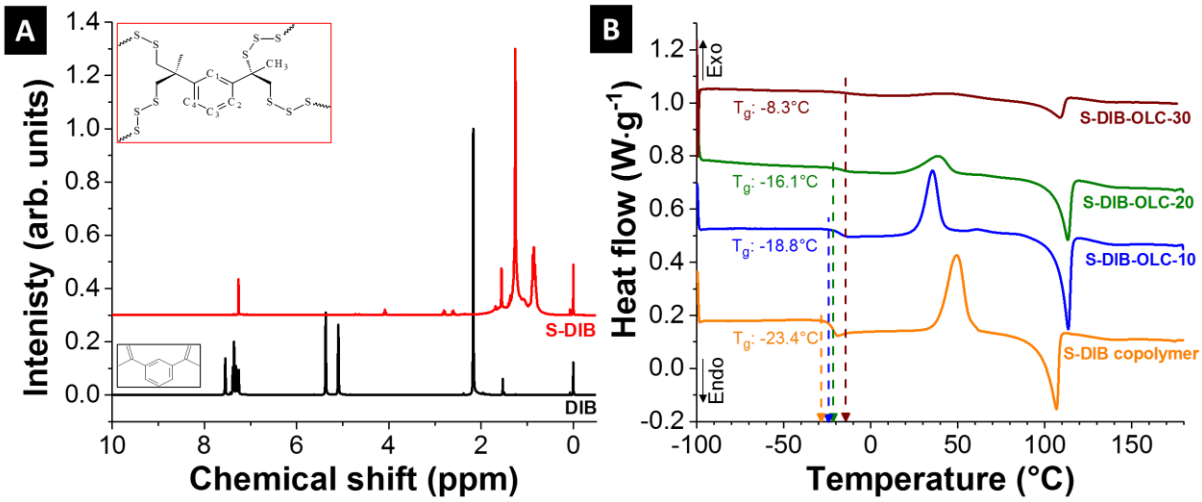


**Figure 2**: $^{1}$H NMR spectra of 1,3-diisopropenylbenzene (DIB) and S-DIB copolymer, (B) differential scanning calorimetry thermograms of sulfur copolymer and its carbon onion hybrids.

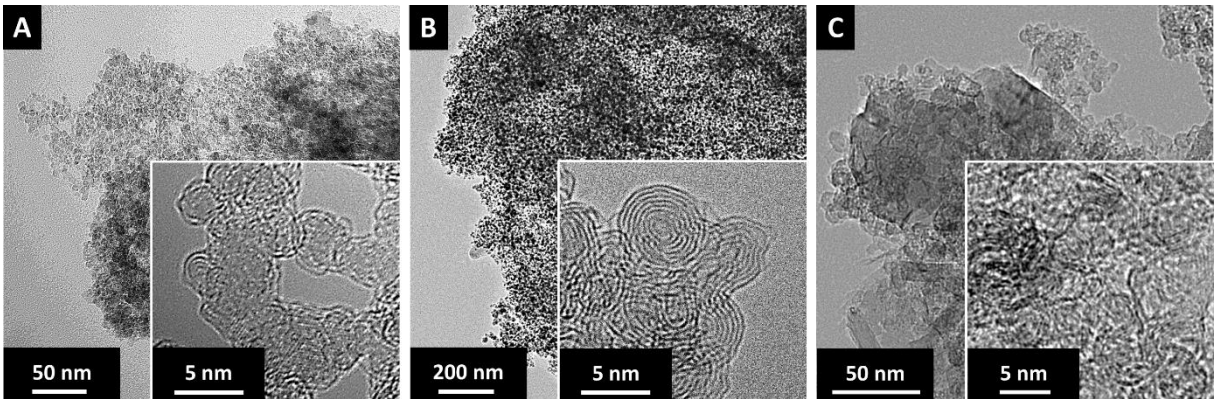


**Figure 3**: High resolution TEM micrographs at different magnifications of (A) nanodiamond particles, (B), carbon onions, and (C) images of S-DIB copolymer / carbon onion hybrid material with 30 mass% carbon onion loading. TEM images of other hybrid compositions are provided in *Supporting Information* **Figure S1**.

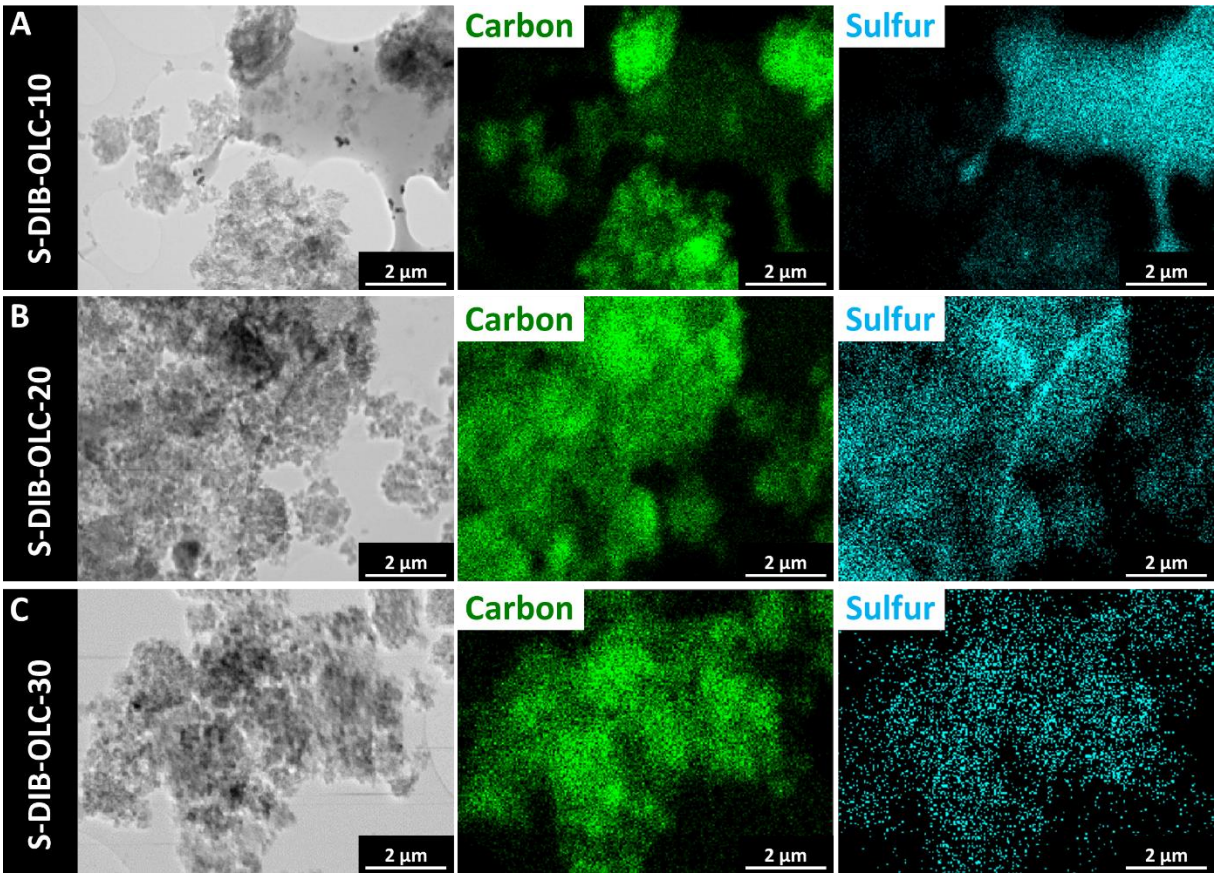


**Figure 4**: Transmission electron micrographs of OLC-sulfur copolymer hybrids and their corresponding elemental maps by EDX.

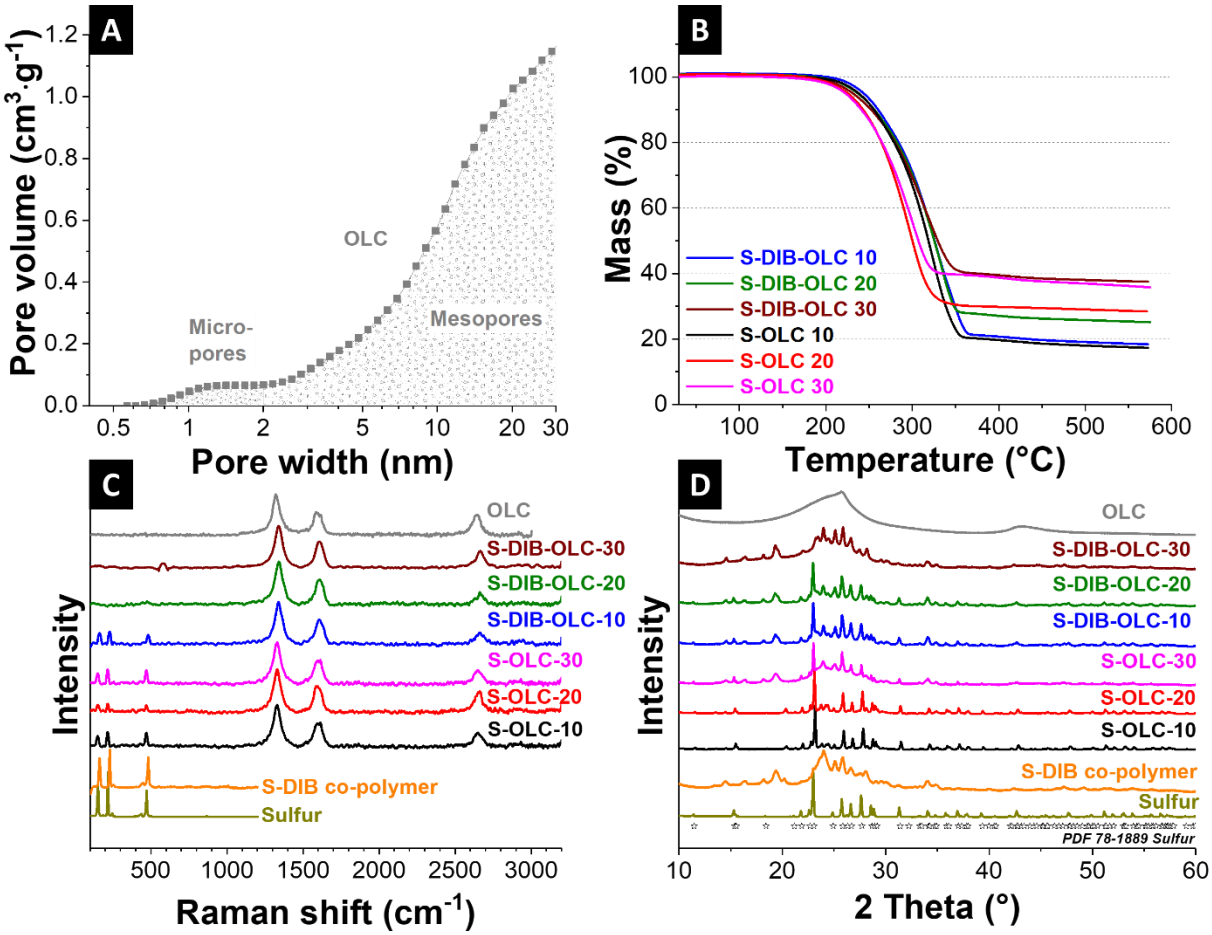


**Figure 5**: (A) Cumulative pore size distribution per volume of carbon onions (dry powder) calculated with quenched-solid density functional theory from nitrogen gas sorption isotherms recorded at a temperature of -196 °C. (B) Thermogravimetric analysis, (C) Raman spectra, and (D) X-ray diffractograms of carbon onions and corresponding sulfur hybrids.

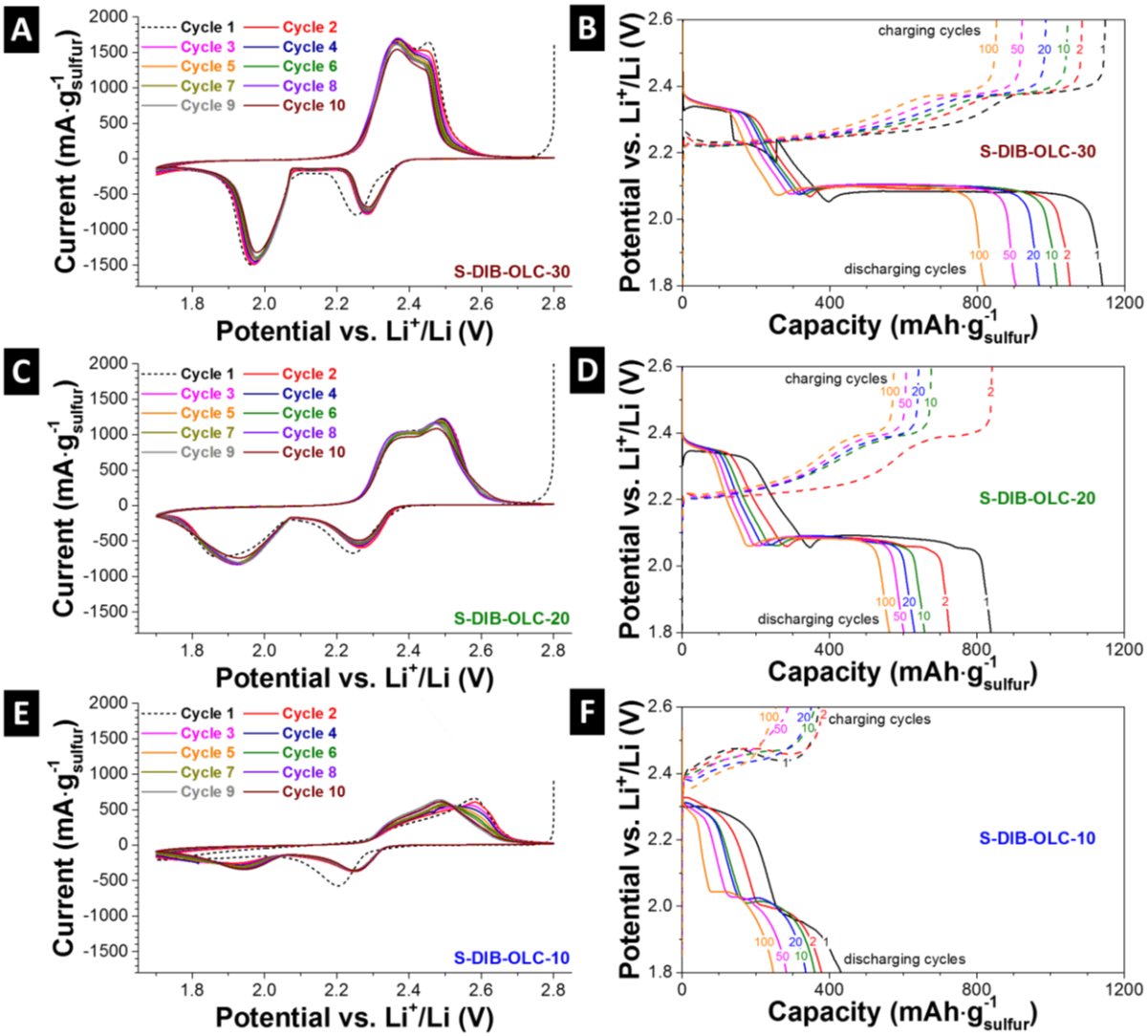


**Figure 6**: Cyclic voltammograms (3-electrode set-up) at a rate of 0.1 mV $s^{-1}$ and galvanostatic charge/discharge profiles (2-electrode set-up in 2032 coin cells) at 336 mA $g^{-1}$ (0.2 C) for charging and 168 mA $g^{-1}$ (0.1 C) for discharging within the potential window of +1.8 V to +2.6 V vs. $Li^+$/Li of (A and B) S-DIB-OLC-30, (C and D) S-DIB-OLC-20, and (E and F) S-DIB-OLC-10. The areal loading of sulfur: 3-5 mg $cm^{-2}$.

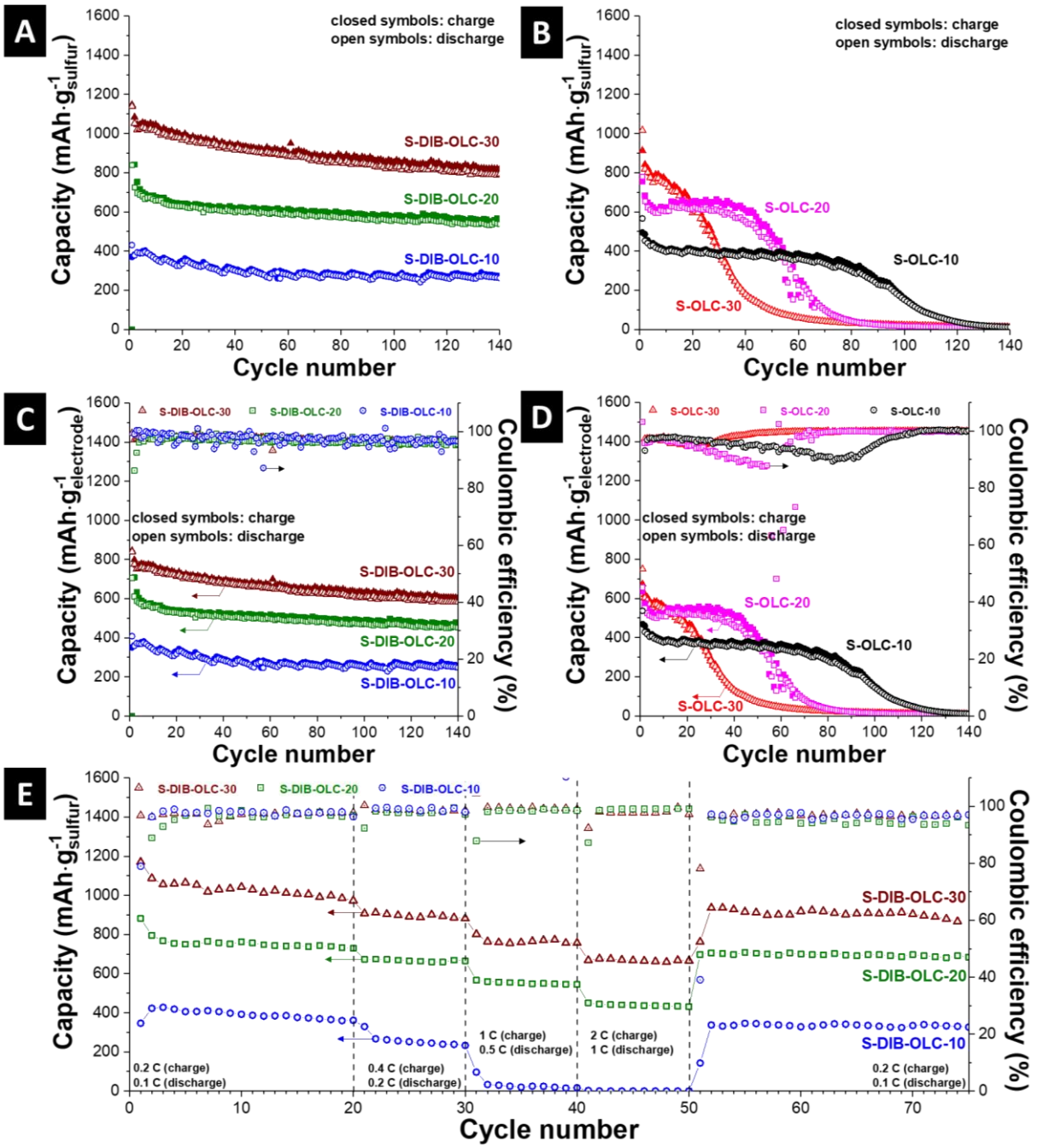


**Figure 7**: Galvanostatic cycling measured in 2032-type coin cells of carbon onion / sulfur hybrids; cycle performance of (A) S-DIB-OLC copolymer hybrid systems, (B) S-OLC melt infused hybrids normalized to sulfur mass, (C and D) the specific capacity values are presented normalized to electrode mass, Coulombic efficiencies are given on the right *y*-axes, and (E) rate handling at different C-rates. The areal loading of sulfur is 3-5 mg $cm^{-2}$.

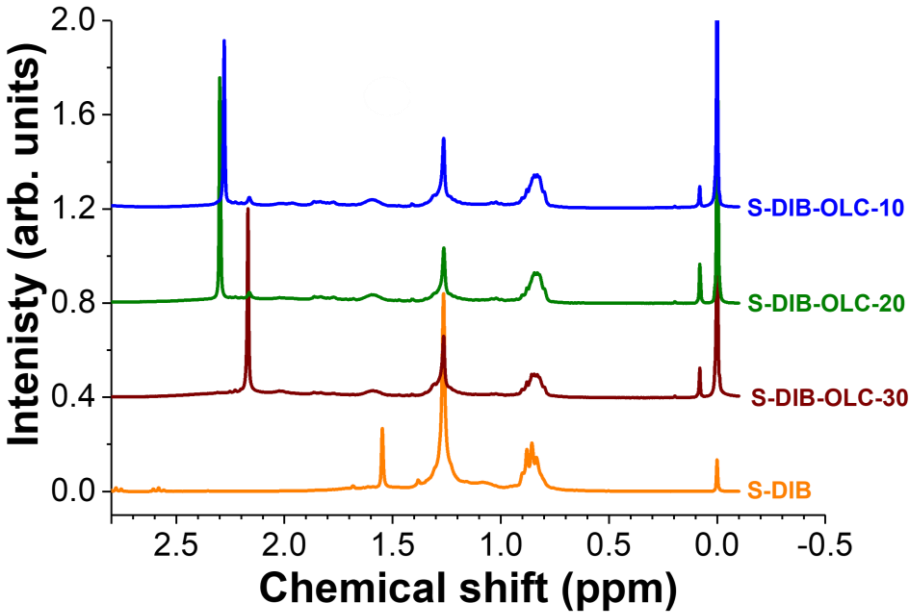


**Figure 8**: $^{1}H$ Nuclear magnetic resonance spectra of pristine S-DIB copolymer and the copolymers extracted from the electrodes after 100 galvanostatic cycles at 0.1 C and corresponding elemental maps measured by EDX.

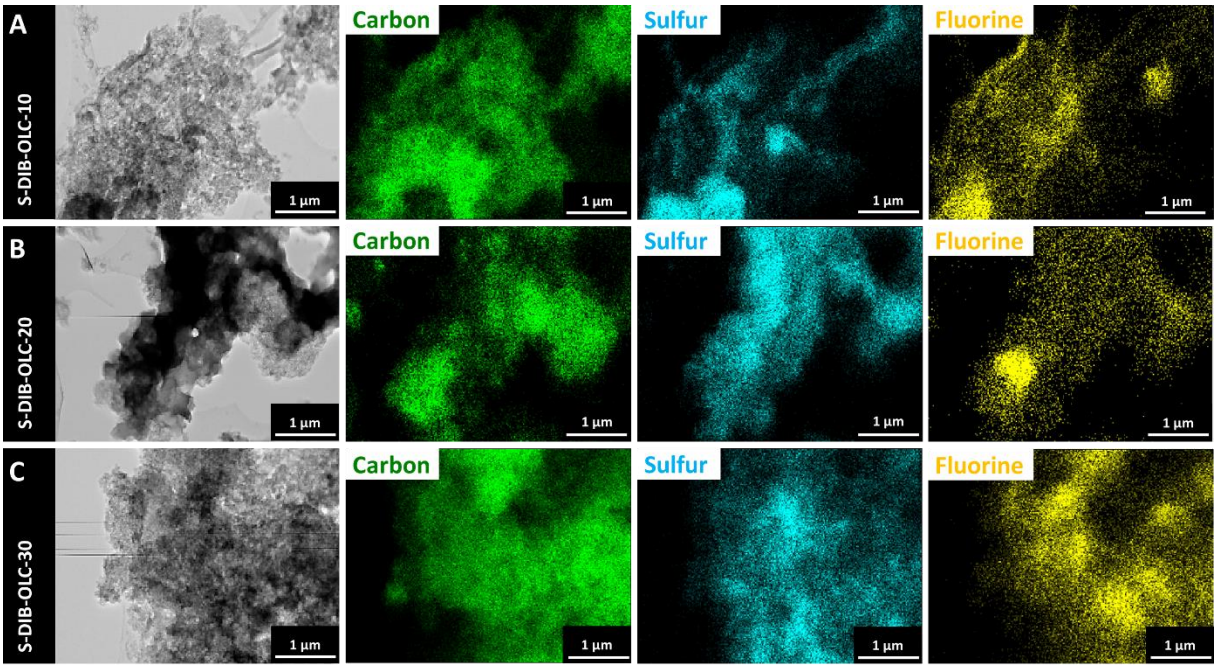


**Figure 9**: Transmission electron micrographs of the electrodes after 100 galvanostatic cycles at 0.1 C and corresponding elemental maps measured by EDX.

## Tables

**Table 1**: Compositions of hybrids with sulfur copolymer and sulfur. All contents are given in mass%.

| | S-DIB-OLC | | S-OLC | |
|---|---|---|---|---|
| | **S-DIB** | **OLC** | **S** | **OLC** |
| **S-DIB-OLC-30** | 70 | 30 | - | - |
| **S-DIB-OLC-20** | 80 | 20 | - | - |
| **S-DIB-OLC-10** | 90 | 10 | - | - |
| **S-OLC-30** | - | - | 70 | 30 |
| **S-OLC-20** | - | - | 80 | 20 |
| **S-OLC-10** | - | - | 90 | 10 |

**Table 2**: Quantification of sulfur content (in mass%) from thermogravimetric analysis and CHNS elemental analysis.

| | S-DIB-OLC | | | S-OLC | | |
|---|---|---|---|---|---|---|
| | **S-DIB-OLC-30** | **S-DIB-OLC-20** | **S-DIB-OLC-10** | **S-OLC-30** | **S-OLC-20** | **S-OLC-10** |
| **TGA** | 64 | 75 | 82 | 63 | 72 | 83 |
| **CHNS** | 65±0.7 | 76±0.6 | 86±0.3 | 64±0.6 | 83±0.8 | 90±0.1 |

**Table 3**: Raman spectroscopy results. FWHM: full-width at half maximum.

| | **Position D-band ($cm^{-1}$)** | **Position G-band ($cm^{-1}$)** | **FWHM D-band ($cm^{-1}$)** | **FWHM G-band ($cm^{-1}$)** | **$I_D/I_G$** |
|---|---|---|---|---|---|
| OLC | 1323 | 1596 | 40.4 | 33.8 | 1.2 |
| S-DIB-OLC-30 | 1340 | 1608 | 50.4 | 40.6 | 1.2 |
| S-DIB-OLC-20 | 1342 | 1610 | 45.6 | 32.2 | 1.4 |
| S-DIB-OLC-10 | 1340 | 1609 | 42.6 | 33.8 | 1.3 |
| S-OLC-30 | 1328 | 1599 | 58.8 | 33.6 | 1.7 |
| S-OLC-20 | 1329 | 1596 | 58.7 | 34.5 | 1.7 |
| S-OLC-10 | 1328 | 1599 | 58 | 32 | 1.8 |

**Table 4:** Electrical conductivity measurements via four-point-probe.

| | **Conductivity ($10^{-2}$ S·$cm^{-1}$)** |
|---|---|
| S-DIB-OLC-30 | 35.9 |
| S-DIB-OLC-20 | 5.5 |
| S-DIB-OLC-10 | 0.5 |
| S-OLC-30 | 31.5 |
| S-OLC-20 | 5.1 |
| S-OLC-10 | 0.5 |

**Table 5:** Electrochemical performances based on areal sulfur loading for selected carbon / sulfur electrodes in comparison to this work. In all reports, metallic Li was used as anode. Used abbreviations: FLG = few-layered graphene; PrGO-S = partially reduced graphene oxide-sulfur; VGCF = vapor grown carbon fiber; CNT = carbon nanotubes; DME = dimethoxyethane; DOL = 1,3-dioxolane; LiTFSI = Li salt of bis(trifluoromethanesulfonyl)imide; PEGDME = polyethylene glycol dimethyl ether; TEGDME = tetraethylene glycol

| **Cathode** | **Surface area ($m^2 \cdot g^{-1}$)** | **Sulfur loading ($mg.cm^{-2}$)** | **Electrolyte** | **Specific capacity ($mAh \cdot g^{-1}_{sulfur}$)** | | | **Potential window** | **C-rate** | **Ref.** |
|---|---|---|---|---|---|---|---|---|---|
| | | | | **Cycle 5** | **Cycle 50** | **Cycle 100** | | | |
| Carbon onion / sulfur hybrid cathodes via inverse vulcanization | ca. 400 | 3-4 | 1 M LiTFSI in 1:1 (v/v) DME/DOL + 0.25 M $LiNO_3$ | ca. 1032 (S-DIB-OLC-30) | ca. 905 (S-DIB-OLC-30) | ca. 880 (S-DIB-OLC-30) | 1.8-2.6 V | 0.1 C | This work - |
| 3-D FLG / PrGO-S electrodes | Unknown | 1.2 | 1 M LiTFSI in 1:1 (v/v) DME/DOL + 0.25 M $LiNO_3$ | ca. 1030 | ca. 1000 | 980 | 1.8-2.8 V | 0.1 C | Ref.[53] |
| Al–S–VGCF sandwich electrode | Unknown | 2-5 | 1 M LiTFSI in 1:1 (v/v) DME/DOL + 0.15 M $LiNO_3$ | ca. 900 | ca. 650 | ca. 600 | 1.8-2.8 V | 0.03 C (Cycle 1), 0.06 C (Cycle 2-100) | Ref.[54] |
| Hierarchical free-standing CNT paper electrodes | ca. 107 | 6.3-17.3 | 1 M LiTFSI in 1:1 (v/v) DME/DOL + 0.25 M $LiNO_3$ | ca. 900 | ca. 820 | ca. 750 | 1.7-2.8 V | 0.05 C | Ref.[52] |
| Vertically aligned CNTs | Unknown | 0.23-4.76 | 1 M LiTFSI in 1:1 (v/v) DME/DOL + 0.25 M $LiNO_3$ | ca. 890 (60 mass% S) | ca. 650 | ca. 560 | 1.8-2.8 V | 0.2 C | Ref.[55] |
| Small CNTs confined inside a large CNT | ca. 150 | 1.36 | 1 M LiTFSI in 1:1 (v/v) DME/DOL | ca. 1250 | ca. 1100 | ca. 1000 | 1.5-3 V | 0.1 C | Ref.[56] |
| Ordered mesoporous carbon (KOH activated) | ca. 1566 | 0.25 | 1 M LiTFSI in 55:40 (v/v) DME/DOL | ca. 500 (51.5 % S) | ca. 300 | - | 1-3.6 V | | Ref.[57] |
| Citric acid interconnected nanosized KB particles with CNT (5 mass%) and graphene (5 mass%) additive | ca. 800 | 4.7 | 1 M LiTFSI in 1:1 (v/v) DME/DOL + 0.1 M $LiNO_3$ | ca. 820 | ca. 800 | ca. 720 (cycle 90) | 1.7-3 V | 0.05 C (Cycle 1-10), 0.2 C (Cycle 10-90) | Ref.[34] |
| Activated carbon fiber cloth | ca. 2000 | 6.5 | 0.35 M LiTFSI in 1:1 (v/v) DME/DOL + 0.29 M $LiNO_3$ | ca. 1000 | ca. 950 | - | 1.7-2.5 V | 0.09 C | Ref.[18] |
| Inverse opal carbon | ca. 1300 | 2-3 | 1 M LiTFSI in 1:1 (v/v) DME/DOL + 0.25 M $LiNO_3$ | ca. 1650 | ca. 400 | - | 1.5-2.8 V | 0.1 C | Ref.[19] |
| 3D gyroidal carbon (activated) | ca. 2000 | 0.8 | 1 M LiTFSI in TEGDME + 0.15 M $LiNO_3$ | ca. 1100 | ca. 1000 | ca. 830 | 1.5-2.8 V | 0.1 C | Ref.[17] |

**Table 6:** Specific capacity values of carbon onion / sulfur hybrids investigated in this work.

| | **Specific capacity ($mAh \cdot g^{-1}_{sulfur}$)** | | **Specific capacity ($mAh \cdot g^{-1}_{electrode}$)** | |
|---|---|---|---|---|
| | **Cycle 1** | **Cycle 100** | **Cycle 1** | **Cycle 100** |
| S-DIB-OLC-30 | 1150 | 880 | 850 | 630 |
| S-DIB-OLC-20 | 840 | 580 | 705 | 480 |
| S-DIB-OLC-10 | 380 | 270 | 350 | 255 |
| S-OLC-30 | 915 | 22 | 670 | 18 |
| S-OLC-20 | 755 | 20 | 635 | 15 |
| S-OLC-10 | 494 | 155 | 465 | 150 |

**Graphical abstract**